The Active Power Control of Cascaded Multilevel Converter Based Hybrid Energy Storage System

Wei Jiang, *Member, IEEE*, Chengwei Zhu, Chen Yang, Lei Zhang, Shuai Xue, and Wu Chen, *Senior Member, IEEE*

***Abstract*—Because of its simple structure, high power quality and enhanced output voltage, cascaded multilevel converter (CMC) has been utilized as the main circuit of power conversion system of energy storage system. However, it is difficult to adapt CMC to hybrid energy storage system (HESS) because of the asymmetric power distribution problem. This paper proposes a novel topology for CMC-based HESS, in which, an *LC* branch is inserted at the end of cascaded H-bridges as a tuned filter, and an odd-harmonic-hybrid-modulation (OHHM) is further proposed to control the harmonic frequency components to transfer power among different energy storage components through the *LC* branch. The principle of the OHHM technique and the design of the *LC* branch are analyzed, based on which, a joint energy recovery and SOC balancing system is introduced. The principle and control method of the proposed HESS is verified by both the simulations and experiments.**

***Index Terms*—Auxiliary power loop, energy recovery control, hybrid energy storage system (HESS), tuned filter.**

NOMENCLATURE

L_r	Inductance of the *LC* branch.
C_r	Capacitance of the *LC* branch.
R_r	Resistance of the *LC* branch.
v_o	Output voltage of the HESS.
v_{ci}	Output voltage of the *i*th cell.
v_{cif}	Fundamental frequency component in v_{ci}.
v_{cih}	All harmonic components in v_{ci}.
v_{bt}	Terminal voltage of the battery.
v_{ei}	Terminal voltage of the *i*th EDLC.
v_{cir}	Additional resonant component in the *i*th cell.
i_a	Current in auxiliary power loop.
f_a	Resonant frequency of the *LC* branch.
f_m	Fundamental frequency.
f_c	Cutoff frequency of the output filter.
V_{sca}	Amplitude of all resonant components.
v_{sci}	Existing resonant component in the *i*th cell.

Manuscript received April 16, 2018; revised July 30, 2018; accepted November 13, 2018. Date of publication November 20, 2018; date of current version May 22, 2019. This work was supported by the National Natural Science Foundations of China under Award 51877041. Recommended for publication by Associate Editor A. Mertens. *(Corresponding author: Wei Jiang.)*

The authors are with the Jiangsu Provincial Key Laboratory of Smart Grid Technology and Equipment, School of Electrical Engineering, Southeast University, Nanjing 210096, China (e-mail:

reference according to the unbalance states. In [18] and [19], fundamental frequency switching is used to maintain the SOC balance of CMC which is powered by battery, EDLC or fuel cell. In [20], the amplitude of carrier-wave is asymmetrically set to control the output power of each H-bridge, so as to achieve the SOC balance of the system.

Another problem of current customer-side ESS is the selection of energy storage strategies. The normal function of customer-side ESS is energy required, so that batteries with high-energy-density are preferred. However, when an ESS provides emergency power to grid, its transient power output capability is critical. The consequences of using single energy storage technology to achieve all these performances are high cost and large volume, and a desirable solution is to combine different kinds of energy storage components to form a hybrid energy storage system (HESS). For instance, by combing EDLC with the battery in a HESS, the energy capacity and the transient performance can be jointly guaranteed [13]–[16].

Taken together, the HESS using CMC power electronic interface is an ideal choice for customer-side energy storage applications. However, to integrate hybrid energy storage component into a CMC circuit requires the improvement of traditional control approaches since the asymmetrical power distribution among different cascaded cells should be controlled. The customer-side energy storage systems are energy type and the capacity of the system is primarily provided by batteries, therefore, a high voltage battery bank is the main source of the system. Low-voltage, low-capacity EDLC banks act as supplemental sources to provide multiple voltage levels and transient active power output and recovery capabilities. In [23], a hybrid modulation method is proposed to unevenly distribute power between main dc-source and energy storage components. The main dc-source switches at the fundamental frequency and the auxiliary converters connected to energy storage components operate at a higher switching frequency. With this approach, low frequency, high voltage switches can be used in the main converter to interface the high voltage dc-side which consists of series connected batteries. The EDLCs in the auxiliary converters are normally used to cancel the harmonic voltage components of the main converter. When needed, the power distribution between batteries and EDLCs can be configured by controlling the switching angle of the main converter and fundamental voltage amplitudes of the auxiliary ones. Although currents of the cascaded converters are couple, the output power can raise to drive motors during acceleration by increasing the output fundamental voltage component of the auxiliary converters.

However, the energy recovery and SOC balancing of the hybrid modulation based HESS depend on its operation mode. If the energy storage components in auxiliary converters are EDLCs, their terminal voltages could decline rapidly during high-power discharge. In this case, the HESS would not properly operate since the output voltage could not be synthesized. In [25], it is proved that the active power can be exchanged between CMC cells via an auxiliary power loop, which consists of an *LC* branch paralleled with cascaded converters. However, the dual-frequency phase-shifted carrier PWM method proposed in [25] is only effective to CMC-based ESS that consists of symmetric segmented energy storage components. Since the dc sides of HESS are asymmetric, the hybrid modulation method need to be improved to support the auxiliary power loop. Enlightened by this idea, this paper proposes an odd-harmonic-hybrid-modulation (OHHM) is proposed, which introduces a harmonic frequency component into auxiliary converters. By controlling the angle and amplitude of this control variable, the active power can be transferred from the battery to the EDLCs. Meanwhile, with the additional freedom of control, the energy recovery and SOC balancing of the EDLCs can be achieved without affecting the major active power output of the system. Therefore, the control range of the HESS can be extended and the merits of power density and energy density energy storage can be fully developed.

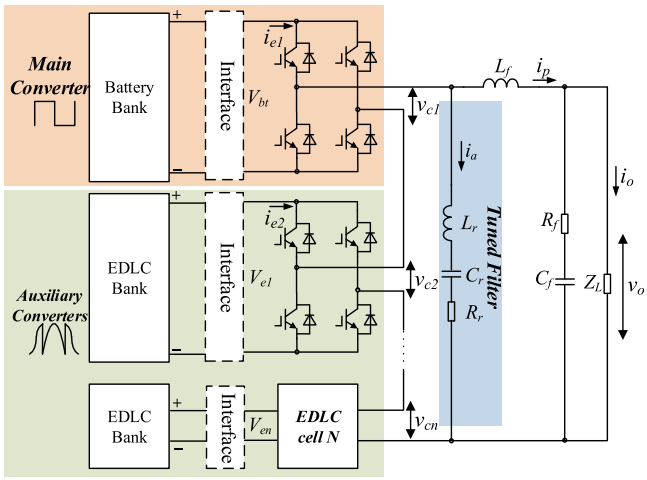

Fig. 1. Topology of proposed ACMC-based ESS.

The rest of this paper is organized as follows: after the introduction section, the CMC-based HESS and the OHHM techniques are introduced in Section II. In Section III, the active power control principle in auxiliary power loop is analyzed and the design of the filters is given. In Section IV, the energy recovery and SOC balancing control strategies are introduced. In Section V, the proposed system is first simulated in a MATLAB/Simulink simulation platform and then implemented on a 5-kW hybrid energy storage test bed. Simulation and experimental results are presented to verify the effectiveness of the proposed system. Finally, Section VI concludes the paper.

II. System Description of the HESS and the OHHM

A. System Description

The proposed CMC-based battery-EDLC HESS is shown in Fig. 1. Since this paper focuses on introducing the OHHM and the auxiliary power loop based power transfer, the single phase system is analyzed. In this configuration, the HESS has one battery source and *N* EDLC sources. These energy storage sources are cascaded connected through H-bridges. The battery bank serves as the dc source of the main cell, and EDLC banks for the other cells. The battery bank and EDLC banks usually contain dc–dc converters for dc-voltage regulation and EDLC frequency-response compensation. Therefore, a dc–dc interface, i.e., bidirectional buck-boost converter or coupling capacitors, is

added between energy storage component and H-bridge, which can help to suppress charge/discharge current ripples. Since the dc–dc interface will not affect the power distribution between H-bridges, its control strategy will not be discussed in this paper. The main difference between the proposed HESS and the drive system investigated in [23] is that an *LC* branch is inserted between the cascaded H-bridges and the output. This *LC* branch helps to realize the active power transfer from battery to EDLCs by creating the auxiliary power loop.

Considering the capacity of the HESS is primarily determined by the battery and the cascaded structure, the voltage of the battery is higher than the EDLCs. Normally, H-bridge 1, whose dc-side is a battery bank, provides most of the active power. The high-voltage-low-frequency switches are used in H-bridge 1, which is defined as the main converter, and they switch at the fundamental frequency to generate a quasi-square wave. Thus, to synthesize the output voltage for the ac load and grid, the other *N* H-bridges, which are defined as auxiliary converters, should generate the difference between sine-wave and quasi-square wave with EDLC dc sources. The fundamental frequency voltage component is only contained in the quasi-square wave. The output voltages of the auxiliary converters, which use EDLCs as dc sources, consist of high frequency harmonic voltage components. Therefore, the auxiliary converters do not provide active power in normal operation mode.

The design of the power and energy capacities of each unit depends on the performance requirement of the HESS. Since the lithium-ion battery has a greater energy density (usually 85–120 W·h/kg) than the valve-regulated lead-acid battery (about 40 W·h/kg). Therefore, the usage of high-energy density lithium-ion battery in H-bridge 1 can effectively reduce the size of the system. If the HESS is designed to work in a long time in high-power mode when EDLC banks provide some of the active power, the size of the HESS will increase because the ELDCs have even lower energy-density (about 10 W·h/kg).

By assuming the output voltages of EDLC cells are symmetric, we have

$$v_o(t) = V_o \sin(\omega_0 t) = v_{c1}(t) + \sum_{i=2}^{n} v_{ci}(t) \tag{1}$$

where v_{c1} is the quasi-square wave voltage of H-bridge 1 and $v_{ci}\,(i = 2, \ldots, N)$ is the supplement wave voltages of the other H-bridges. V_o is the amplitude of the output sine wave and ω_0 is the fundamental angular frequency.

The waveforms of $v_{c1}(t)$ and $v_{ci}(t)\,(i = 2, \ldots, N)$ is depicted in Fig. 2. By introducing θ as the fundamental phase shift angle of v_{c1}, we have

$$v_{c1}(t) = \begin{cases} 0, & t \in (kT, \theta + kT) \cup \left[\left(k+\frac{1}{2}\right)T - \theta, \left(k+\frac{1}{2}\right)T + \theta\right] \\ & \quad \cup \left[(k+1)T - \theta, (k+1)T\right] \quad k = 0, 1, 2 \ldots \\ V_{bt}, & t \in \left[\theta + kT, \left(k+\frac{1}{2}\right)T - \theta\right] \\ -V_{bt}, & t \in \left[\left(k+\frac{1}{2}\right)T + \theta, (k+1)T - \theta\right] \end{cases} \tag{2}$$

The Fourier series expansion of v_{c1}(t) is given by

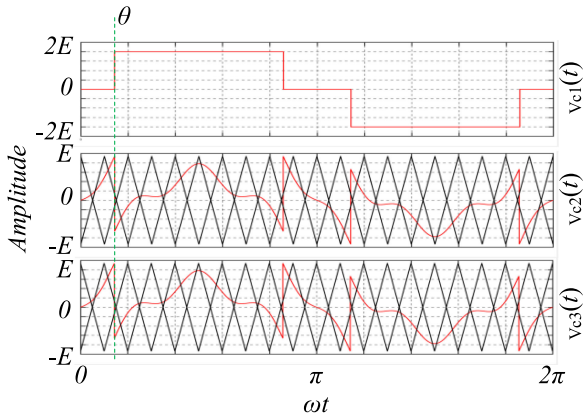

Fig. 2. Voltage waveforms of the H-bridges.

$$\begin{aligned} v_{c1}(t) &= \sum_{n=1,3,5,\ldots}^{\infty} \frac{4V_{bt}}{n\pi} \cos(n\omega_0\theta) \sin(n\omega_0 t) \\ &= v_{c1f}(t) + v_{c1h}(t) \end{aligned} \tag{3}$$

where V_{bt} is the voltage of the battery, $v_{c1f}(t)$ is the fundamental sine wave voltage in $v_{c1}(t)$, and $v_{c1h}(t)$ is the sum of all odd harmonics in $v_{c1}(t)$.

The supplement wave voltages consists of two components: first, sine component which is in phase with $v_o(t)$ and determines the real power output of the EDLCs; second, harmonic component which cancels v_{c1h} in the v_{c1}. If we assume the supplement wave voltages are symmetrical, there is

$$\begin{aligned} v_{ci}(t) &= \frac{1}{N}\left[v_o(t) - v_{c1}(t)\right] = \frac{1}{N}\left[V_{cif}\sin(\omega_0 t)\right. \\ &\quad \left. - \sum_{n=3,5,\ldots}^{\infty} \frac{4V_{bt}}{n\pi} \cos(n\omega_0\theta) \sin(n\omega_0 t)\right] \\ &= v_{cif}(t) + v_{cih}(t) \quad i = 2, \ldots, N \end{aligned} \tag{4}$$

where V_{cif} is the amplitude of the fundamental sine wave component of $v_{ci}(t)\,(i = 2, \ldots, N)$.

There are abundant odd harmonic in the quasi-square wave voltage v_{c1}, however, one of them is only selected to be the resonant frequency of the *LC* branch f_a. According to the orthogonal power flow theory, if the active power generated from the nonsinusoidal voltage *v*(*t*) and current *i*(*t*) is considered to be the average value of the product of their instantaneous values, the power produced by different frequency components are orthogonal to each other, where *v*(*t*), *i*(*t*), and average active power *P* can be expressed by

$$v(t) = V_0 + \sum_{n=1}^{\infty} \sqrt{2} V_n \cos(n\omega t + \theta_n) \tag{5}$$

$$i(t) = I_0 + \sum_{n=1}^{\infty} \sqrt{2} I_n \cos(n\omega t + \varphi_n) \tag{6}$$

$$P = V_0 I_0 + \sum_{n=1}^{\infty} V_n I_n \cos(\theta_n - \varphi_n). \tag{7}$$

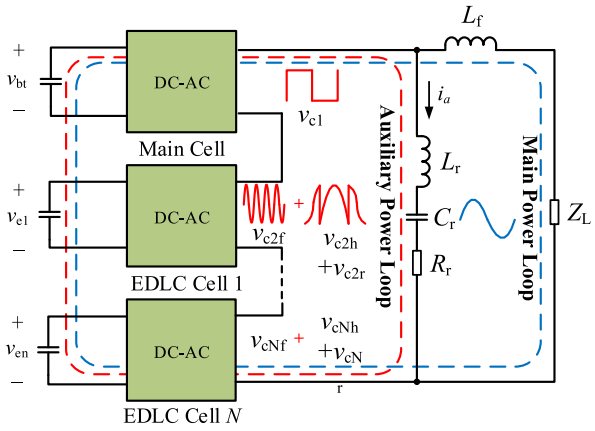

Fig. 3. Main and auxiliary power loops in the HESS.

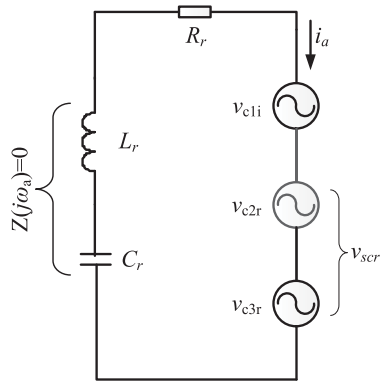

Fig. 4. Equivalent circuit of the auxiliary power loop.

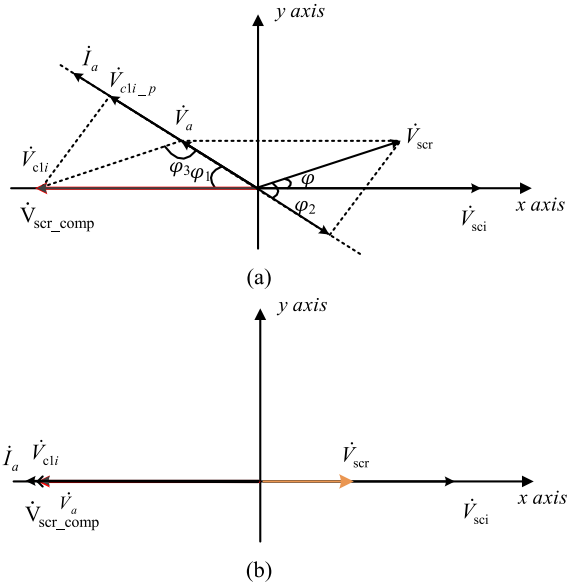

Fig. 5. Phase diagram of the auxiliary power loop. (a) General situation. (b) Maximum power exchange point (MPEP).

Based on this theory, the power resulting from the resonant frequency voltage and current will be restricted in the loop formed with L_r, C_r, R_r, and the cascaded H-bridges and will not affect the output power of the system. Fig. 3 illustrates the two separate power loops. An additional resonant frequency component $v_{cir}(t)$ $(i = 2, \ldots, N)$ is added to $v_{cih}(t)$ to control the angle and amplitude of the current $i_a(t)$ in the auxiliary power loop. The power EDLCs absorb from the loop are determined by the phase lag between $i_a(t)$ and $v_{cir}(t)$. Meanwhile, the sum of quasi-square wave $v_{c1}(t)$ and $v_{ci}(t)$ is the output voltage of the main power loop. Since the resonant frequency component is unwanted in the output voltage, its existence in the auxiliary power will not affect the main power loop.

In the proposed HESS, auxiliary power loop is used to transfer power from the battery to EDLCs since EDLCs' terminal voltage declines rapidly with high-power discharge. Meanwhile, by controlling the power transfers of different cells, the SOC balancing can be realized.

B. OHHM Principle

The direction and amplitude of the auxiliary power flow are determined by the selected frequency components in $v_{ci}(t)$. In this section, an OHHM is proposed for this purpose. To simplify the analysis, the following assumptions are made.

1) The HESS contains one battery cell and two EDLC cells.
2) The dc voltages of all energy storage components are constant.
3) Current flow at the auxiliary frequency is kept in the auxiliary power loop.
4) The equivalent impedance of the series *LC* branch at f_a is pure resistance $(Z(j\omega_a) = R_r)$.
5) All switches, diodes, inductor, and capacitor are ideal components.

With above-mentioned assumptions, the equivalent circuit of the auxiliary loop is shown in Fig. 4, where L_r, C_r and R_r forms the tuned filter and i_a is the auxiliary frequency current flowing in the loop. v_{c1i} represents the ith harmonic of V_{c1}, whose frequency equals the resonant frequency of the tuned filter, given by

$$v_{c1i}(t) = \frac{4V_{bt}}{i\pi}\cos(\omega_i\theta)\sin(\omega_i t) \tag{8}$$

where ω_i is the angular frequency of the selected odd harmonics.

The resonant frequency components of v_{c2} and v_{c3}, that is, v_{c2r} and v_{c3r}, are used to control the power transfers in auxiliary power loop, given by

$$v_{c2r}(t) = v_{c3r}(t) = \frac{1}{2}V_{sca}\sin(\omega_a t + \varphi) \tag{9}$$

$$v_{scr}(t) = v_{c2r}(t) + v_{c3r}(t) = V_{sca}\sin(\omega_a t + \varphi) \tag{10}$$

where V_{sca} is the amplitude of the resonant frequency voltage component and φ_1 is the phase lag to the *x*-axis.

As shown in Fig. 5(a), $\dot{V}_{sci}$ is the existing resonant frequency harmonic in v_{c2} and v_{c3}, which equals $-\dot{V}_{c1i}$. A voltage vector $\dot{V}_{scr\_comp}$ which equals $\dot{V}_{c1i}$ is added to compensate $\dot{V}_{\rm sci}$. $\dot{V}_{c1i}$, $\dot{V}_{scr}$, and $\dot{I}_a$ are vectors of v_{c1i}, v_{scr}, and i_a, respectively. $\dot{V}_{scr}$ is the controllable resonant frequency voltage component used to change the power transfers in an auxiliary power loop. $\dot{V}_{c1i\_p}$

and $\dot{V}_{scr\_p}$ are the active components of $\dot{V}_{c1i}$ and $\dot{V}_{scr}$, which are in phase with $\dot{I}_a$. φ_2 is the phase difference between $\dot{V}_{scr}$ and $\dot{V}_{scr\_p}$. $\dot{V}_a$ is the vector sum of $\dot{V}_{scr}$ and $\dot{V}_{c1i}$ and determines $\dot{I}_a$. Using the geometrical analysis, we have

$$\begin{aligned}\cos(\varphi_2) &= \cos(\varphi+\varphi_1) = \cos(\pi-\varphi_3)\\ &= -\cos\varphi_3 = -\frac{V_a^2+V_{sca}^2-V_{c1}^2}{2V_aV_{sca}} \qquad (11)\\ V_a^2 &= V_{c1}^2+V_{sca}^2-2V_{c1}V_{sca}\cos\varphi\\ &= \left[\frac{4V_{bt}}{i\pi}\cos(\omega_i\theta)\right]^2+V_{sca}^2-2\frac{4V_{bt}}{i\pi}\\ &\quad |\cos(\omega_i\theta)|\,V_{sca}\cos\varphi\\ &= \frac{4V_{bt}}{i\pi}|\cos(\omega_i\theta)|\left[\frac{4V_{bt}}{i\pi}|\cos(\omega_i\theta)|-2V_{sca}\cos\varphi\right]\\ &\quad +V_{sca}^2 \qquad (12)\end{aligned}$$

where V_a is the amplitude of $\dot{V}_a$, and V_{c1} is the amplitude of $\dot{V}_{c1i}$

The active power generated from $\dot{V}_{c1i}$ and $\dot{I}_a$ consists of two components: P_e is the active power absorbed by the EDLC cells, which is the product of $\dot{V}_{scr\_p}$ and $\dot{I}_a$, and P_{loss} is the power loss on R_r, which is resulted from $\dot{V}_a$ and $\dot{I}_a$. We have

$$P_e = V_{sca}\cos\varphi_2 I_a \qquad (13)$$

$$P_{\text{loss}} = \frac{V_a^2}{R_r}. \qquad (14)$$

From (8)–(14), we have (15) and (16) shown at the bottom of this page, when $\varphi=0$, we can obtain the power exchange with certain V_{sca} can be obtained as follows:

$$P_e = V_{sca}\left[\frac{4V_{bt}}{i\pi}|\cos(\omega_i\theta)|-V_{sca}\right]/R_r \qquad (17)$$

$$\begin{aligned}P_{\text{loss}} &= \frac{\frac{4V_{bt}}{i\pi}|\cos(\omega_i\theta)|\left[\frac{4V_{bt}}{i\pi}|\cos(\omega_i\theta)|-2V_{sca}\right]+V_{sca}^2}{R_r}\\ &= \frac{\left[\frac{4V_{bt}}{i\pi}|\cos(\omega_i\theta)|-V_{sca}\right]^2}{R_r}. \qquad (18)\end{aligned}$$

The P_{e_0} to P_{loss_0} diagram is depicted in Fig. 6. It is easy to find out that when setting $V_{sca}=\frac{2V_{bt}}{i\pi}|\cos(\omega_i\theta)|$ we can achieve

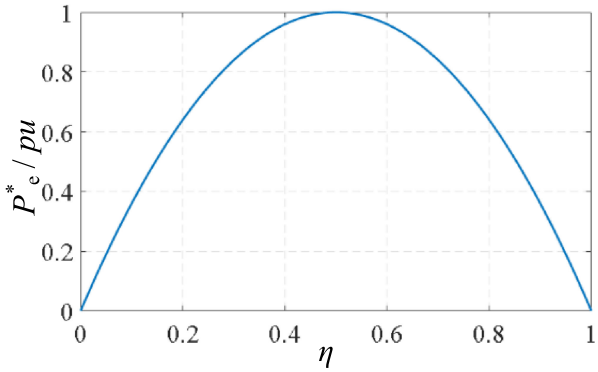

Fig. 6. Efficiency versus power exchange (pu).

the maximum power exchange point (MPEP), given by

$$P_{e\_\text{mpep}} = \frac{\left[\frac{2V_{bt}}{i\pi}\cos(\omega_i\theta)\right]^2}{R_r} \qquad (19)$$

$$P_{\text{loss\_mpep}} = \frac{\left[\frac{2V_{bt}}{i\pi}\cos(\omega_i\theta)\right]^2}{R_r}. \qquad (20)$$

The phase diagram of MPEP is shown in Fig. 5(b).

III. Power Transfer and Resonant Frequency Selection Analysis

A. Power Transfer Analysis

From (3) and (4), it can be seen that both the output voltages of the battery cell and the EDLC cells contain a fundamental sine wave component. The real power distribution between them is determined by the fundamental sine wave amplitude ratio r_p, which is given by

$$r_p = \frac{V_o - V_{c1f}}{V_{c1f}} \qquad (21)$$

where $V_{c1f}=\frac{4V_{bt}}{\pi}|\cos(\omega_i\theta)|$.

Since the battery is energy density energy storage, we can assume V_{bt} is constant during charge/discharge processes. However, EDLC's dc voltage varies with its SOC and affects the power distribution range. By defining V_{ei} as the dc voltage of the ith EDLC, when EDLC cells operate synthetically, the minimum requirement of V_{ei} is to be equal to the peak of $v_{c1h}(t)$,

$$\begin{aligned}P_e &= V_{sca}\cos\varphi_2\frac{V_a}{R_r} = V_{sca}\left(-\frac{V_a^2+V_{sca}^2-V_{c1}^2}{2V_aV_{sca}}\right)\frac{V_a}{R_r} = \frac{V_{c1}^2-V_a^2-V_{sca}^2}{2R_r}\\ &= \frac{\left\{\left(\frac{4V_{bt}}{i\pi}\cos(\omega_i\theta)\right)^2-\left(\frac{4V_{bt}}{i\pi}|\cos(\omega_i\theta)|\left[\frac{4V_{bt}}{i\pi}|\cos(\omega_i\theta)|-2V_{sca}\cos\varphi\right]+V_{sca}^2\right)-V_{sca}^2\right\}}{2R_r}\\ &= V_{sca}\left[\frac{4V_{bt}}{i\pi}|\cos(\omega_i\theta)|\cos\varphi-V_{sca}\right]/R_r \qquad (15)\end{aligned}$$

$$P_{\text{loss}} = \frac{V_a^2}{R_r} = \frac{\frac{4V_{bt}}{i\pi}|\cos(\omega_i\theta)|\left[\frac{4V_{bt}}{i\pi}|\cos(\omega_i\theta)|-2V_{sca}\cos\varphi\right]+V_{sca}^2}{R_r} \qquad (16)$$

and consequently, the odd harmonic in $v_{c1}(t)$ can be canceled. In this way

$$V_{c1f} = V_o \tag{22}$$

$$\begin{aligned} V_{ei\_\min} &= V_{bt} - V_{c1f}\sin(\omega_0\theta) \\ &= V_{bt} - \frac{4V_{bt}}{\pi}\left|\cos(\omega_i\theta)\right|\sin(\omega_0\theta)\ \ \omega_0\theta\epsilon\left(0,\frac{\pi}{2}\right) \end{aligned} \tag{23}$$

where $V_{ei\_\min}$ is the minimal requirement of V_{ei}.

Since the dc voltage of EDLCs will decline during the discharge process, the initial value of $V_{e1}+V_{e2}$ should be higher than V_{ei}_min. Meanwhile, if the requirement of the HESS is to provide maximum power $P_{\max}$ and considering the maximum discharge current of the battery is $I_{\max}$, which is determined by maximum discharge rate and the capacitance of the battery. In this working condition, the peak of output voltage $V_{o\_\max}$ of the HESS becomes

$$V_{o\_\max} = \frac{\sqrt{2}P_{\max}}{I_{\max}}. \tag{24}$$

When $V_{o\_\max}$ exceeds $\frac{4V_{bt}}{\pi}$, which is the maximum amplitude of $v_{c1f}(t)$, EDLC cells should provide active power by injecting fundamental frequency voltage into v_{c1} and v_{c2}. In this way, the fundamental sine wave amplitude ratio is

$$\begin{aligned} r_{p\_\max} &= \frac{V_{o\_\max} - V_{c1f}}{V_{c1f}} = \frac{\frac{\sqrt{2}P_{\max}}{I_{\max}} - V_{c1f}}{V_{c1f}} \\ &= \frac{\sqrt{2}P_{\max} - V_{c1f}I_{\max}}{V_{c1f}I_{\max}}. \end{aligned} \tag{25}$$

Considering the minimum requirement V_{ei}_min and the fundamental frequency component in v_{c1} and v_{c2}, the required dc voltage of the EDLCs must satisfy (26) shown at the bottom of this page.

If the HESS is designed to output $P_{\max}$ for T_c and there is no way to transfer power from the battery to EDLCs, the total energy provided by EDLCs is

$$W_{\text{ELDC}} = P_{\max}T_c - \frac{2\sqrt{2}V_{bt}}{\pi}\left|\cos(\omega_i\theta)\right|I_{\max}T_c. \tag{27}$$

Consequently, the requirement of the initial dc voltages of the EDLCs is

$$\left[\sum_{i=1}^{2}V_{ei}\right]_{\text{init\_min}} = 2\sqrt{\left(\frac{W_{\text{EDLC}}}{\sum_{i=1}^{2}C_i} + \left(\sum_{i=1}^{2}V_{ei}\right)_{\min}\right)^2} \tag{28}$$

where C_i $(i=1,2)$ is the capacitance of the *i*th EDLC bank.

With an increase in $P_{\max}$, a larger number of EDLC cells should be connected in series to achieve a sufficient amount of initial dc voltage, and the cost, volume, and control complexity of the HESS also increase. However, with the proposed OHHM and auxiliary power loop technology, power transfer from battery to EDLCs via an auxiliary power loop can significantly reduce the requirement of initial dc voltages of the EDLCs.

If the auxiliary power loop is activated, the power EDLCs can absorb from the battery is

$$W_e = P_{e\_0}T_c = \frac{V_{sca}\left|\left[\frac{4V_{bt}}{i\pi}\left|\cos(\omega_i\theta)\right|\cos\varphi - V_{sca}\right]\right|T_c}{R_r}. \tag{29}$$

Therefore, the initial dc voltages of the EDLCs can reduce to

$$\left[\sum_{i=1}^{2}V_{ei}\right]'_{\text{init\_min}} = 2\sqrt{\left(\frac{W_{\text{EDLC}} - W_e}{\sum_{i=1}^{2}C_i} + \left(\sum_{i=1}^{2}V_{ei}\right)_{\min}\right)^2}. \tag{30}$$

Equation (30) indicates that when W_{EDLC} and W_e are comparable, the decrease in the initial dc voltage requirement of EDLCs is significant. On the other hand, with a certain maximum dc voltage of EDLCs, the propose OHHM is also able to reduce the capacitance retirement of the EDLCs.

B. Resonant Frequency Analysis and Tuned Filter Design

The selection of the resonant frequency of the *LC* branch and the design of the tuned filter is discussed in this section. The *LC* branch consists of three passive components: L_r, C_r, and R_r. The *LC* branch provides a low impedance path to the current at the resonant frequency and high impedance paths to the fundamental frequency and other harmonic frequency currents. Ideally, there is

$$\omega_i L_r = \frac{1}{\omega_i C_r} \tag{31}$$

where $\omega_i = 2\pi f_{\text{i}}$, and f_i is the frequency of the selected *i*th harmonic. The following concerns should be taken into account for the selection of the harmonic frequency:

1) The power loss caused by the fundamental frequency voltage on the *LC* components.
2) The power transfer capability of the auxiliary power loop.
3) The potential shift of actual parameters of resonant inductor and capacitor.

First, the relationship between the power loss and the power transfer ability of the *LC* branch is analyzed in order to select the odd harmonic frequency as its resonant frequency.

$$\begin{aligned} \left[\sum_{i=1}^{2}V_{ei}\right]_{\min} &= \max\left(V_{bt} - \frac{4V_{bt}}{\pi}\left|\cos(\omega_i\theta)\right|\sin(\omega_0\theta), V_{o\_\max} - V_{bt}\right) \\ &= \begin{cases} V_{bt} - \frac{4V_{bt}}{\pi}\left|\cos(\omega_i\theta)\right|\sin(\omega_0\theta) & V_{o\_\max} < V_{bt} - \frac{4V_{bt}}{\pi}\left|\cos(\omega_i\theta)\right|\sin(\omega_0\theta) \\ V_{o\_\max} - V_{bt} & V_{o\_\max} \geq V_{bt} - \frac{4V_{bt}}{\pi}\left|\cos(\omega_i\theta)\right|\text{in}(\omega_0\theta) \end{cases} \end{aligned} \tag{26}$$

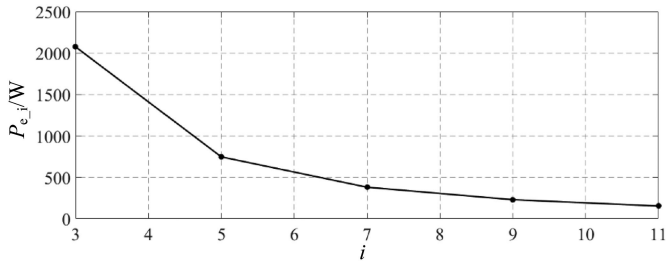

Fig. 7. P_{e_i} to P_{loss_i} diagram.

The impedance of the *LC* at the fundamental frequency can be expressed by

$$Z_r = R_r + \mathrm{j}L_r\left(\omega_0 - \frac{\omega_i^2}{\omega_0}\right). \tag{32}$$

Therefore, the power loss at ω_0 can be calculated as follows:

$$P_{\text{loss}\_i} = \frac{\left(\frac{4V_{bt}}{\pi}\right)^2}{\sqrt{\left[R_r^2 + \left(\omega_0' L_r\right)^2\right]}}\cos\varphi_0 \tag{33}$$

where $\omega_0' = \frac{(i\omega_0)^2}{\omega_0} - \omega_0 = (i^2-1)\omega_0$, and $\varphi_0 = \arctan\frac{\omega_0' L_r}{R_r}$.

Meanwhile, according to (19), when the *i*th odd harmonic frequency is selected as the resonant frequency of the *LC* branch, its maximum power transfer ability is

$$P_{e\_i} = \frac{\left[\frac{2V_{bt}}{i\pi}\right]^2}{R_r}. \tag{34}$$

The relationship between P_{e_i} and P_{loss_i} is depicted in Fig. 7. The simulation parameters are: $R_r = 0.1\,\Omega$, $L_r = 50\,\text{mH}$, and $V_{bt} = 24\,\text{V}$. As shown in Fig. 7, the maximum power transfer decreases logarithmically with *i* increases. Note that, the performance of the output filter should also be considered when selecting the harmonic order, and this will be discussed in the following section.

With a certain resonant frequency in hand, there are different combinations of L_r and C_r. The design of L_r will also affect the power loss caused by the fundamental frequency voltage. According to (33), larger L_r should be selected to decease P_{loss_i}. However, if the manufacturing error ΔL is considered, the actual impedance at ω_i is

$$Z_{rr} = R_r + j\omega_a\Delta L = \sqrt{R_r^2 + (\omega_a\Delta L)^2}\angle\Delta\varphi \tag{35}$$

where $\Delta\varphi = \arctan\frac{\omega_a\Delta L}{R_r}$.

In this way, the auxiliary current can be expressed as (36) shown at the bottom of this page.

From (36), we observe that the parameter error causes decreases in both the amplitude and the phase shift of the auxiliary current, and the power transfer range in the auxiliary power loop also diminishes. The power transfer range in the auxiliary power loop will also diminish. With certain maximum power transfer requirement and power loss restrictions, the tuned filter can be optimally designed according to [24].

C. Output Filter Design and Resonant Frequency Selection

Since the voltage at *i*th harmonic added to the output of EDLC cells cannot be canceled, together with that in the quasi-square wave, the output of the cascaded H-bridges can be expressed as follows:

$$\begin{aligned} v_s(t) &= v_{c1}(t) + v_{c2}(t) + v_{c3}(t) \\ &= \frac{4V_{bt}}{\pi}\sin(\omega_0 t) + \frac{2V_{bt}}{i\pi}\sin(\omega_i t + \pi). \end{aligned} \tag{37}$$

The target of the output filter is to eliminate the second term in (37). The characteristic impedance of the second-order low-pass filter used as the output filter is

$$R = \sqrt{\frac{L_f}{C_f}}. \tag{38}$$

The cutoff frequency of the output filter is

$$f_c = \frac{\omega_c}{2\pi} = \frac{1}{2\pi\sqrt{L_f C_f}}. \tag{39}$$

With (38) and (39), there is

$$L_f = R/(2\pi f_c) \tag{40}$$

$$C_f = \frac{L_f}{R^2} = 1/(2\pi f_c R). \tag{41}$$

From (40) and (41), it is easy to observe that that the design of L_f and C_f depend on the characteristic impedance *R*, which is related to the power loss. According to the Impedance matching principle, the load R_L should be equal to the output impedance, i.e., $Z_{c2} = \frac{\mathrm{R}}{\sqrt{1-f_m^2/f_c^2}}$. Consequently, the characteristic impedance in the passband is pure resistance and the power loss on the filter is eliminated. In our design, the cutoff frequency of the output filter is set to be $f_c = 100\,\text{Hz}$ and the fundamental output frequency $f_m = 50\,\text{Hz}$. In this way, we have $R_L = Z_{c2} = \frac{2}{\sqrt{3}}R$. Accordingly, both L_f and C_f can be calculated with (40) and (41). For example, when $R_L = 7\,\Omega$, $R \approx 6\ \Omega$ and $f_c = 100\,\text{Hz}$, the filter parameters can be chosen as follows:

$$L_f = \frac{R}{2\pi f_c} = 9.55\ \text{mH} \tag{42}$$

$$C_f = \frac{1}{2\pi f_c R} = 265\,\mu\text{F}. \tag{43}$$

The bode diagram of this designed filter is provided in Fig. 8. It can be seen that the fundamental components in (37) are able to pass the filter without any attenuation. The filtering performance against the 3rd–7th harmonics is simulated as shown in Fig. 9.

$$\dot{I}_a = \frac{\dot{V}_a}{Z_{rr}} = \frac{\frac{4V_{bt}}{i\pi}\cos(\omega_i\theta)\left[\frac{4V_{bt}}{i\pi}\cos(\omega_i\theta) - 2V_{sca}\cos\varphi\right] + V_{sca}^2}{\sqrt{R_r^2 + (\omega_a\Delta L)^2}}\angle\pi - \varphi_1 - \Delta\varphi \tag{36}$$

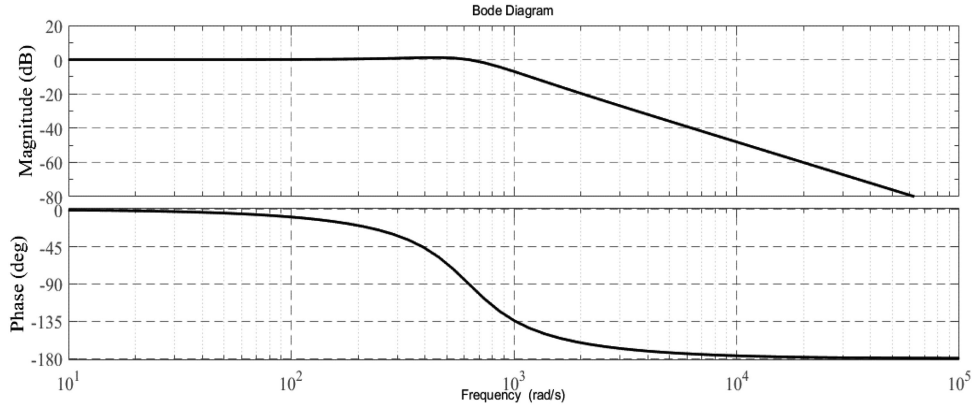

Fig. 8. Bode diagram of the output filter.

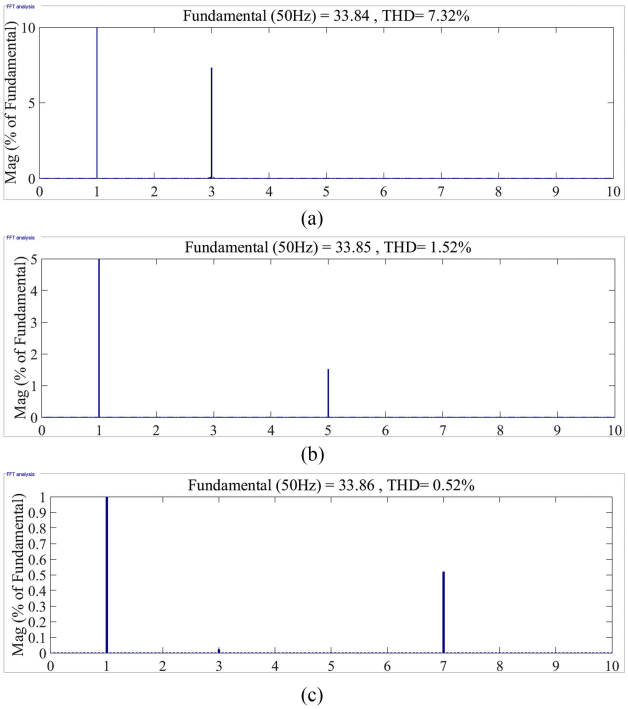

Fig. 9. FFT simulation result of the output filter. (a) $f_a = 150$ Hz. (b) $f_a = 250$ Hz. (c) $f_a = 350$ Hz.

According to the harmonic regulation [25], the 5th and 7th harmonics can be selected as the resonant frequency of the *LC* branch.

IV. Control System Design

A. Energy Recovery and SOC Balancing Control

Since EDLCs possess limited energy densities, after a high power output, their terminal voltages tend to decline. When their terminal voltages decline to a certain level, the HESS fails, since the desired output voltage cannot be synthesized. Traditional energy recovery control uses the phase-shift between the output current and fundamental frequency voltage of EDLC cells to generate a reserve power flow to charge them. However, this approach highly depends on the operation state of the HESS and the energy recovery power is coupled with the output power. Particularly, when the HESS is on standby, the energy recovery process cannot be activated. On the other hand, because of the inconsistency of capacities, SOCs of EDLCs deviate during the charge/discharge process. By considering that unbalanced SOC values have a negative effect on the system, SOC balancing control among EDLC cells should be included in the control system.

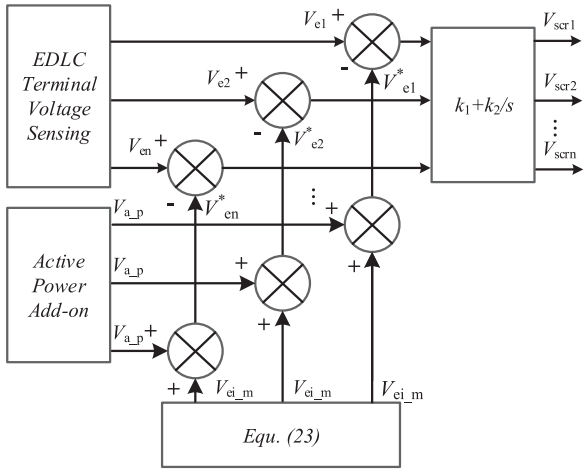

Fig. 10. Diagram of the simultaneous control of energy recovery and SOC balancing.

As discussed, the OHHM technology can be used to transfer power from the battery to EDLCs. With this desirable property, both the energy recovery control and the SOC balancing control can be realized, based on asymmetrically power flows control of different EDLCs via an auxiliary power loop, whose main control variable is the dc voltage of EDLCs. The diagram of the energy recovery and the SOC balancing control is shown in Fig. 10.

As discussed in Section III-A, the minimal requirement of the EDLC terminal voltages V_{ei_m} is equal to the peak of $v_{c1h}(t)$. Meanwhile, when the EDLCs provide active power, an additional dc voltage component V_{a_p} will be added to the minimal requirement. With a certain power distribution ratio r_p, V_{a_p} can

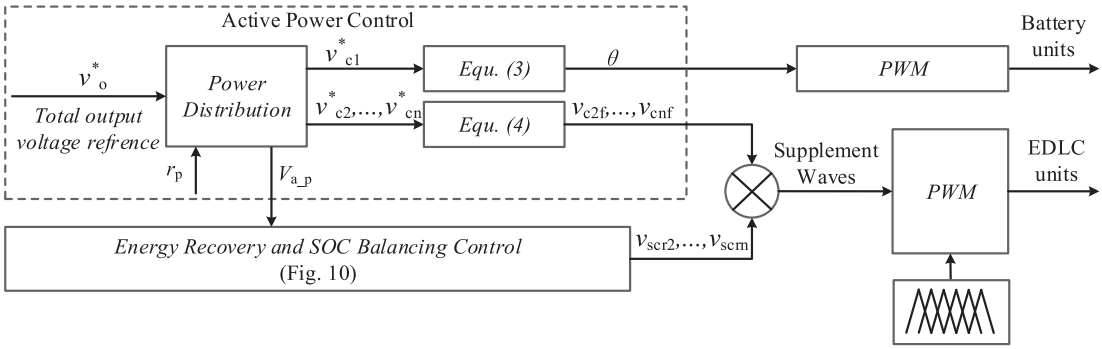

Fig. 11. Diagram of control system of the HESS.

TABLE I
SIMULATION PARAMETER

Parameters	Symbol	Value
Battery		
Rated capacity	C_b	10 AH
Rated voltage	V_{bt}	24 V
ESR	R_{esr_b}	0.5 Ω
EDLC		
Rated voltage	V_{sc}	12 V
Voltage range	V_{cr}	0-20 V
Rated capacity	C_{sc}	5 F
ESR	R_{esr_sc}	0.1 Ω
Frequency		
Carrier frequency	f_c	2500 Hz
Auxiliary frequency	f_a	250 Hz
Fundamental frequency	f_m	50 Hz
LC Branch		
Inductance of tuned filter	L_r	4.5 mH
Capacitance of tuned filter	C_r	90 uF
Resistance of tuned filter	R_r	0.1 Ω
Output Filter		
Inductance of output filter	L_f	9.55 mH
Capacitance of output filter	C_f	265 uF
Converter		
Load	R_L	7 Ω
Output voltage	V_o	32.8 V

be determined by

$$V_{a\_p} = V_o - V_{bt} - V_{ei\_m}. \tag{44}$$

The sensed dc voltages of EDLCs $v_{e1} \sim v_{en}$ are compared to $V_{ei\_m} + V_{a\_p}$. The differences are compensated with three separate but identical PI controllers. The outputs of the PI controllers are controllable resonant frequency voltages $v_{scr1} - v_{scrN}$. Within this control strategy, the dc voltages of EDLCs will be evenly balanced as the required and the energy recovery and SOC balancing control targets can be achieved synchronously.

B. Control System Design for the HESS

The complete control system diagram of the HESS is shown in Fig. 11. This control system consists of two subsystems: active power control and energy recovery and SOC balancing control. The input of the active power control is the total output voltage reference v_o^*, which can be used to drive a motor or provide emergency power supply. With a certain power distribution ration r_p, the voltage references of battery (v_{c1}^*) and EDLCs $(v_{c2}^*, \ldots, v_{cn}^*)$ at the fundamental frequency can be calculated by using (22) and (23). Meanwhile, the additional dc voltage requirement V_{a_p} can be obtained and sent to energy recovery and SOC balancing control subsystem. If only battery provides active power, the references for EDLCs equal 0. Otherwise, they are superimposed to the outputs of the energy recovery and SOC balancing control subsystem and their summation serves as the reference of supplement waves for the EDLCs. The phase shift angle of the quasi-square wave θ can be determined by v_{c1}^* and (3).

V. SIMULATION AND EXPERIMENTAL RESULTS

In order to verify the proposed topologies and the theoretical analysis, the model of proposed HESS with auxiliary power loop

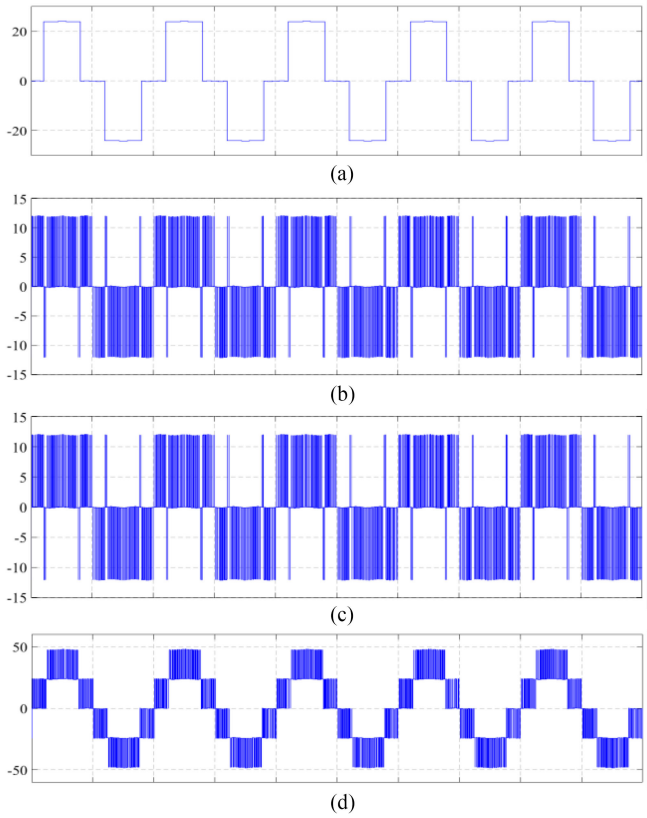

Fig. 12. Voltage waveforms of the H-bridges. (a) V_{c1} (Battery). (b) V_{c2} (EDLC 1). (c) V_{c3} (EDLC 2).

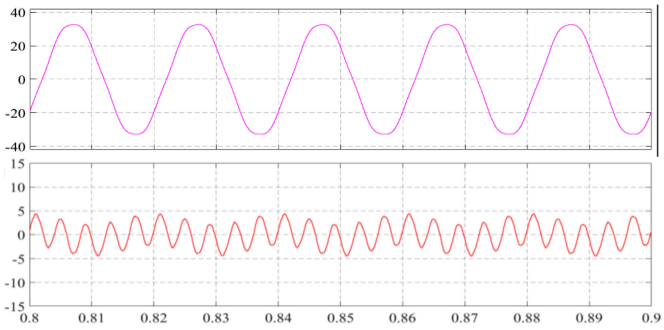

Fig. 13. Output of the HESS. (a) V_o. (b) I_a.

is simulated in the MATLAB/SIMULINK simulation platform. This model consists of one battery and two EDLCs, and 5th harmonic is selected as the resonant frequency of the auxiliary power loop. The detailed parameters are listed in Table I.

In the first stage, the effectiveness of OHHM is considered. Fig. 12 shows the voltage waveforms of the H-bridges of the proposed HESS. As shown in Fig. 12(a), the battery cell outputs a quasi-square wave with a phase shift angle of $\omega_i\theta = \pi/5$. As shown in Fig. 12(b) and (c), the two EDLCs output supplement waves and resonant frequency voltage component v_{scr2}, v_{scr3} with an amplitude $V_{sca} = \frac{2V_{bt}}{i\pi}|\cos(\omega_i\theta)| = 3.056$ V and a phase shift angle $\varphi = 0$. Fig. 12(d) shows their summation, which serves as the output of the cascaded H-bridges. Fig. 13 shows the output voltage and the auxiliary current of the HESS.

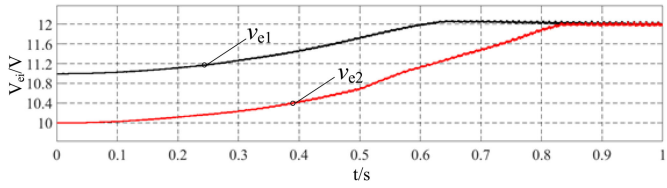

Fig. 14. DC voltages of the EDLCs.

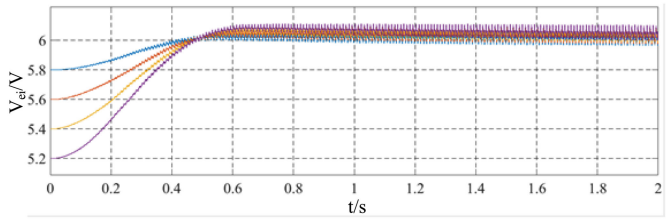

Fig. 15. SOC-balancing control waveforms of four EDLCs.

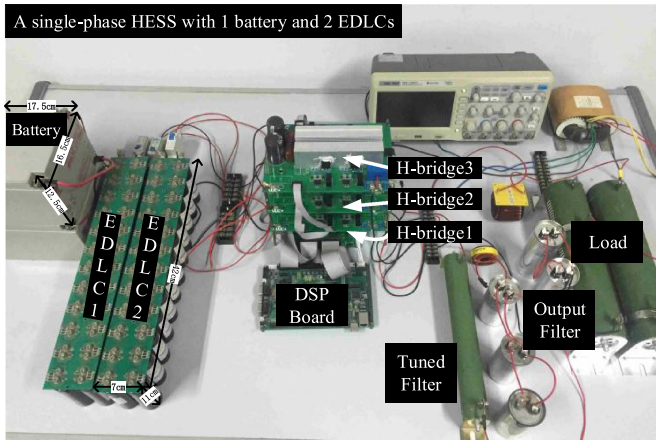

Fig. 16. Prototype with three H-bridges.

As desired, the output voltage is a pure 50-Hz sine wave and the current in auxiliary power loop only contains only a 250-Hz sine component.

In the next stage, the energy recovery and SOC balancing potentialities of the proposed control method is verified. The initial dc voltages of the two EDLCs are 10 V and 11 V, respectively. As shown in Fig. 14, with the proposed energy recovery and SOC balancing control, the EDLCs absorb power from the battery via the auxiliary power loop and recover their terminal voltages to rated values. This process will not affect the output of the HESS since the auxiliary power loop is decoupled with the main power loop.

To further prove the effectiveness of the proposed energy recovery and SOC balancing control in multiple EDLC configurations, a HESS with four batteries is simulated. The EDLCs are of different initial SOC values centered around 90%. As shown in Fig. 15, the dc voltages of EDLCs are gradually balanced along with their respective discharge. During the SOC balancing process, each EDLC unit decides the transferred power from the battery according to their dc voltages.

To verify the proposed topology and the PWM technology, A 5-kW prototype is designed, as shown in Fig. 16.

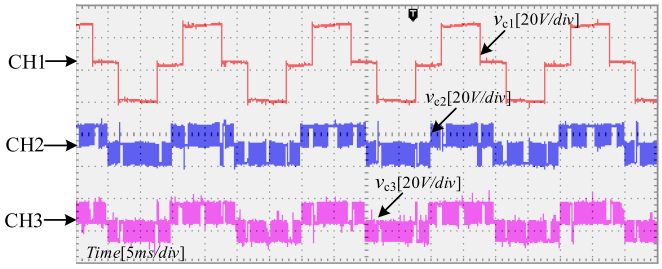

Fig. 17. Voltage waveforms of v_{c1}–v_{c3} in the open-loop experiment environment.

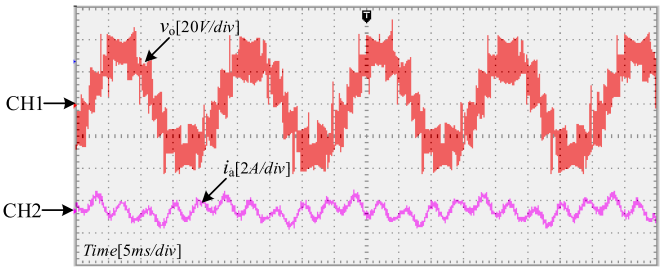

Fig. 18. Output voltage waveform of the cascaded H-bridges and the current waveform in the proposed *LC* branch.

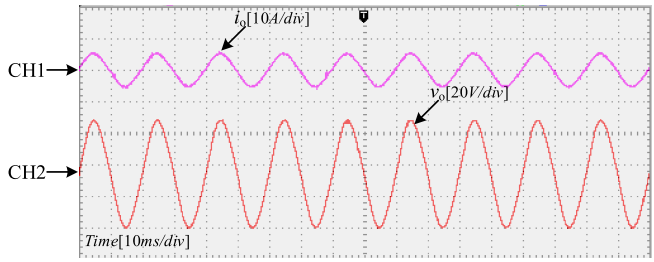

Fig. 19. Waveforms of both the voltage and the current at the fundamental frequency on the ac load.

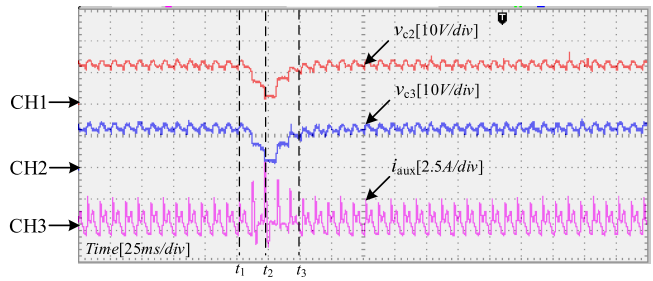

Fig. 20. Terminal voltages of EDLCs and the battery in energy recovery experiment.

The prototype consists of one 24 V/10 A·h battery and two 12 V/1F EDLCs, whose system parameters are: $L_r = 4.5\,\text{mH}$, $C_r = 90\,\mu\text{F}$, $R_r = 0.1\,\Omega$, $L_f = 10\,\text{mH}$, $C_f = 250\,\mu\text{F}$, $R_L = 6\,\Omega$, $V_c = 24\,\text{V}$, $f_m = 50\,\text{Hz}$, $f_a = 250\,\text{Hz}$, and $f_c = 2500\,\text{Hz}$. The FF200R17KE3 MOSFET are used in all H-bridges. The sizes of the battery and EDLC units are marked in the picture. The control system shown in Fig. 11 is implemented in TI TMS320F28335 digital signal processor, which is responsible for sampling voltages/currents and generating real time parameters for OHHM.

In the experiment, the effectiveness of the proposed OHHM method is first investigated in an open-loop control environment. The fundamental phase shift angle θ is set to $\frac{\pi}{5}$. The 5th harmonics component with an amplitude of $V_{sca} = \frac{2V_{bt}}{i\pi}|\cos(\omega_i\theta)| = 3.056$ V and a phase shift angle of 0° is superimposed into the supplement wave voltages v_{c2} and v_{c3}. The voltage waveforms of v_{c1}–v_{c3} is shown in Fig. 17.

The output voltage waveform of the cascaded H-bridges and the current waveform in *LC* branch are shown in Fig. 18. It can be seen that the summation of v_{c1}–v_{c3} is a multilevel PWM wave at the fundamental frequency. Meanwhile, because of the frequency-selection characteristic, the *LC* branch mainly includes the 5th harmonics current. The current frequency characteristic in the *LC* branch offers EDLC cells the opportunity to absorb power from the battery unit under the control strategy introduced in Section IV-A. Fig. 19 shows both the voltage and the current waveforms on the ac load. The designed output filter successfully eliminates the harmonic components in the output voltage of the cascaded H-bridges. In this way, the output voltage v_o and current i_o contain the 50-Hz sinusoidal component only.

The efficiency of the system is given by

$$\eta_s = \frac{W_p}{W_e} = 0.923 \tag{45}$$

where W_p is the measured energy consumption on the load and W_e is the total energy provided by the battery and the EDLCs. Therefore, the 7.7% power loss includes the loss of passive components of the auxiliary power loop, the switching loss, and the loss of the output filter.

The energy recovery and SOC balancing strategy are also integrated into the control platform to investigate the effectiveness of the power exchange in the auxiliary power loop within the OHHM. In the experiment, two EDLCs are first charged to their rated voltage 12 V. At time t_1, a sudden high power output occurs and the terminal voltages of the EDLCs decline to 2 V in 20 ms. At time t_2, the energy recovery control is activated and the EDLCs absorb power from the battery cell via the auxiliary power loop. At time t_3, the terminal voltages of the EDLCs rise to 12 V. Because of the SOC balancing strategy, their recovery processes are synchronous. This process is recorded and shown in Fig. 20, where CH3 is the dc current of the battery in this experiment. There is an obvious current surge from t_1 to t_3 since the battery undertakes high power output from t_1 to t_2 and provide recovery power to EDLCs from t_1 to t_3. The dc current change in the battery justifies that the recovery energy is provided by the battery via the auxiliary power loop.

VI. Conclusion

In this paper, a novel hybrid energy storage system that contains one battery source and multiple EDLC sources has been proposed. The main innovation is to use the specific harmonic frequency component in the quasi-square voltage to transfer

power to the series-connected EDLCs from the battery through the auxiliary power loop. To precisely utilize the power loop generated from the voltage and the current at a selected frequency, an OHHM method has been proposed to control both the direction and the capacity of the power through an auxiliary power loop by adjusting both the amplitude and the phase shift angle of the selected harmonic voltage. The selection of the harmonic order and the maximum power exchange are analyzed to facilitate the design of the *LC* branch. The energy recovery and SOC balancing control of the ELDCs based on proposed topology and OHHM has been verified through simulations and experiments.

REFERENCES

[1] L. Baruschka and A. Mertens, "Comparison of cascaded H-bridge and modular multilevel converters for BESS application," in *Proc. IEEE Energy Convers. Cong. Expo.*, 2011, pp. 909–916.

[2] P. W. Hammond, "A new approach to enhance power quality for medium voltage AC drives," *IEEE Trans. Ind. Appl.*, vol. 33, no. 1, pp. 202–208, Jan./Feb. 1997.

[3] L. G. Franquelo, J. Rodriguez, J. I. Leon, S. Kouro, R. Portillo, and M. A. M. Prats, "The age of multilevel converters arrives," *IEEE Ind. Electron. Mag.*, vol. 2, no. 2, pp. 28–39, Jun. 2008.

[4] K. A. Corzine, M. W. Wielebski, F. Z. Peng, and J. Wang, "Control of cascaded multilevel inverters," *IEEE Trans. Power Electron.*, vol. 19, no. 3, pp. 732–738, May 2004.

[5] S. Kouro *et al.*, "Recent advances and industrial applications of multilevel converters," *IEEE Trans. Ind. Electron.*, vol. 57, no. 8, pp. 2553–2580, Aug. 2010.

[6] H. Akagi, S. Inoue, and T. Yoshii, "Control and performance of a transformerless cascade PWM STATCOM with star configuration," *IEEE Trans. Ind. Appl.*, vol. 43, no. 4, pp. 1041–1049, Jul./Aug. 2007.

[7] R. H. Osman, "A medium-voltage drive utilizing series-cell multilevel topology for outstanding power quality," in *Proc. 34th IAS Annu. Meeting Conf. Rec. IEEE Ind. Appl. Conf. (Cat. No.99CH36370)*, 1999, pp. 2662–2669, vol. 4.

[8] D. Montesinos-Miracle, M. Massot-Campos, J. Bergas-Jane, S. Galceran-Arellano, and A. Rufer, "Design and control of a modular multilevel DC/DC converter for regenerative applications," *IEEE Trans. Power Electron.*, vol. 28, no. 8, pp. 3970–3979, Aug. 2013.

[9] C. M. Young, N. Y. Chu, L. R. Chen, Y. C. Hsiao, and C. Z. Li, "A single-phase multilevel inverter with battery balancing," *IEEE Trans. Ind. Electron.*, vol. 60, no. 5, pp. 1972–1978, May 2013.

[10] F. Z. Peng, "A generalized multilevel inverter topology with self voltage balancing," *IEEE Trans. Ind. Appl.*, vol. 37, no. 2, pp. 611–618, Mar./Apr. 2001.

[11] M. Vasiladiotis and A. Rufer, "Balancing control actions for cascaded H-bridge converters with integrated battery energy storage," in *Proc. 15th Eur. Conf. Power Electron. Appl.*, 2013, pp. 1–10.

[12] F. Z. Peng, J.-S. Lai, J. McKeever, and J. VanCoevering, "A multilevel voltage-source converter system with balanced DC voltages," in *Proc. 26th Annu. IEEE Power Electron. Specialists Conf.*, 1995, pp. 1144–1150, vol. 2.

[13] Z. Zheng, K. Wang, L. Xu, and Y. Li, "A hybrid cascaded multilevel converter for battery energy management applied in electric vehicles," *IEEE Trans. Power Electron.*, vol. 29, no. 7, pp. 3537–3546, Jul. 2014.

[14] M. D. Manjrekar, P. K. Steimer, and T. A. Lipo, "Hybrid multilevel power conversion system: A competitive solution for high-power applications," *IEEE Trans. Ind. Appl.*, vol. 36, no. 3, pp. 834–841, May/Jun. 2000.

[15] J. Rodriguez, J.-S. Lai, and F. Z. Peng, "Multilevel inverters: A survey of topologies, controls, and applications," *IEEE Trans. Ind. Electron.*, vol. 49, no. 4, pp. 724–738, Aug. 2002.

[16] Z. Du, L. M. Tolbert, J. N. Chiasson, B. Ozpineci, H. Li, and A. Q. Huang, "Hybrid cascaded H-bridges multilevel motor drive control for electric vehicles," in *Proc. 37th IEEE Power Electron. Specialists Conf.*, 2006, pp. 1–6.

[17] L. Maharjan, S. Inoue, H. Akagi, and J. Asakura, "State-of-charge (SOC)-balancing control of a battery energy storage system based on a cascade PWM converter," *IEEE Trans. Power Electron.*, vol. 24, no. 6, pp. 1628–1636, Jun. 2009.

[18] C. M. Young, N. Y. Chu, L. R. Chen, Y. C. Hsiao, and C. Z. Li, "A single-phase multilevel inverter with battery balancing," *IEEE Trans. Ind. Electron.*, vol. 60, no. 5, pp. 1972–1978, May 2013.

[19] L. A. Tolbert, F. Z, Peng, T. Cunnyngham, and J. N. Chiasson, "Charge balance control schemes for cascade multilevel converter in hybrid electric vehicles," *IEEE Trans. Ind. Electron.*, vol. 49, no. 5, pp. 1058–1064, Oct. 2002.

[20] Z. Zheng, K. Wang, L. Xu, and Y. Li, "A hybrid cascaded multilevel converter for battery energy management applied in electric vehicles," *IEEE Trans. Power Electron.*, vol. 29, no. 7, pp. 3537–3546, Jul. 2014.

[21] I. Krastevm, N. Mukherjee, P. Tricoli, and S. Hillmansen, "New modular hybrid energy storage system and its control strategy for a fuel cell locomotive," in *Proc. 17th Eur. Conf. Power Electron. Appl. (EPE'15 ECCE-Eur.)*, 2015, pp. 1–10.

[22] N. Mukherjee and D. Strickland, "Control of second-life hybrid battery energy storage system based on modular boost-multilevel buck converter," *IEEE Trans. Ind. Electron.*, vol. 62, no. 2, pp. 1034–1046, Feb. 2015.

[23] L. Liu, H. Li, S. H. Hwang, and J. M. Kim, "An energy-efficient motor drive with autonomous power regenerative control system based on cascaded multilevel inverters and segmented energy storage," *IEEE Trans. Ind. Appl.*, vol. 49, no. 1, pp. 178–188, Jan./Feb. 2013.

[24] W. Jiang, L. Huang, L. Zhang, H. Zhao, L. Wang, and W. Chen, "Control of active power exchange with auxiliary power loop in a single-phase cascaded multilevel converter-based energy storage system," *IEEE Trans. Power Electron.*, vol. 32, no. 2, pp. 1518–1532, Feb. 2017.

[25] General Administration of Quality Supervision, Inspection and Quarantine of the People's Republic of China, "Quality of electric energy supply Harmonics in public supply network," 1993.

Wei Jiang (M'12) received the B.S., M.S., and Ph.D. degrees in electrical engineering from Southeast University, Nanjing, China, in 2004, 2008, and 2012, respectively.

He is currently an Associate Professor with the School of Electrical Engineering, Southeast University. His research interests include the application of power electronics in distributed generation systems, energy storage systems, and power quality control.

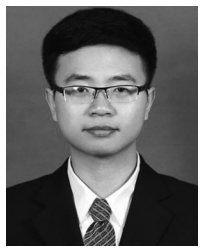

Chengwei Zhu was born in Anhui, China, in 1994. He received the B.S. degrees from The China University of Mining and Technology, Xuzhou, China, in 2017, and is currently working toward the M.S. degree in electrical engineering at Southeast University, Nanjing, China.

His research interests include cascaded multilevel converters and control of energy storage systems.

Chen Yang was born in Anhui, China, in 1994. He received the B.S. degree, in 2016, from the Southeast University (SEU), Nanjing, China, where she is currently working toward the M.S. degree in electrical engineering.

His research interest focuses on application of energy storage in power systems.

Lei Zhang was born in Anhui, China, in 1994. He received the B.S. degree from Anhui University, Hefei, China, in 2015, and is currently working toward the M.S. degree in electrical engineering from Southeast University, Nanjing, China.

His research interest focuses on cascaded multilevel converters.

Shuai Xue received the B.S. degree from Qingdao University, Qingdao, China, in 2016. He is currently working toward the M.S. degree in electrical engineering from Southeast University, Nanjing, China.

His research interests include cascaded multilevel converters and control of power converters.

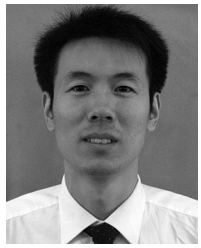

Wu Chen (S'05–M'12–SM'17) received the B.S., M.S., and Ph.D. degrees in electrical engineering from the Nanjing University of Aeronautics and Astronautics, Nanjing, China, in 2003, 2006, and 2009, respectively.

From 2009 to 2010, he was a Senior Research Assistant with the Department of Electronic Engineering, City University of Hong Kong, Kowloon, Hong Kong. In 2010–2011, he was a Postdoctoral Researcher in Future Electric Energy Delivery and Management Systems Center, North Carolina State University, Raleigh, NC, USA. Since September 2011, he has been an Associate Research Fellow with the School of Electrical Engineering, Southeast University, Nanjing, China, and since May 2016, he has been a Professor. His main research interests include soft-switching converters, microgrids, and power electronic applications.